crystals

MDPI

Article

Fab Fragment of V_HH-Based Antibody Netakimab: Crystal Structure and Modeling Interaction with Cytokine IL-17A

Olga Kostareva [1,*], Ilya Kolyadenko [1], Andrey Ulitin [2], Victoria Ekimova [2], Stanislav Evdokimov [2], Maria Garber [1], Svetlana Tishchenko [1] and Azat Gabdulkhakov [1]

1 Institute of Protein Research RAS, Institutskaya 4, Pushchino, Moscow 142290, Russia; kolyadenko_ilya@mail.ru (I.K.); garber@vega.protres.ru (M.G.); sveta@vega.protres.ru (S.T.); azat@vega.protres.ru (A.G.)

2 CJSC Biocad, ul.Svyazi., 34-A, p. Strelna, Saint-Petersburg, Leningrad 198515, Russia; ulitin@biocad.ru (A.U.); ekimova@biocad.ru (V.E.); evdokimov@biocad.ru (S.E.)

* Correspondence: oskostareva@gmail.com

Received: 1 March 2019; Accepted: 21 March 2019; Published: 26 March 2019

Abstract: Interleukin 17A (IL-17A) is a proinflammatory cytokine produced by Th17 cells. Antibody BCD-085 (netakimab) against human IL-17A is one of the new inhibitors of this cytokine. In netakimab, the V_H domain is replaced by the V_HH domain of *Lama glama* possessing a long complementarity determining region (CDR-H3) in its heavy chain. Here we demonstrate the high affinity of IL-17A to the Fab fragment of netakimab and to its integral part, the V_HH domain. We have determined the crystal structure of the Fab fragment of netakimab at 1.9 Å resolution. High variability in the orientation of light and heavy chains of the Fab fragment of netakimab was shown, which is determined by the peculiarity of the structural organization of the CDR-H3. As the high conformational plasticity of the molecule hampers modeling the Fab fragment of netakimab complexed to IL-17A, we have carried out modeling the complex between the antigen and the integral part of the Fab fragment, the V_HH domain. We explain the high netakimab Fab fragment affinity for IL-17A by a large number of protein–protein contacts due to additional interactions between CDR-H3 and the cytokine dimer.

Keywords: V_HH domain; Fab fragment; netakimab; crystal structure; complementarity determining regions; interleukin 17A

1. Introduction

Cytokine IL-17A plays a key role in protecting an organism against extracellular bacterial and fungal infections [1]. However, excessive production of this protein is associated with immune-mediated inflammatory and autoimmune diseases (for instance, psoriasis, psoriatic arthritis, rheumatoid arthritis, systemic lupus erythematosus, etc.) [2]. By now, substantial progress has been achieved in the therapy of such diseases, which was associated with the widespread introduction of therapeutic preparations based on anti-IL-17 antibodies [3].

Along with classical antibodies, preparations based on non-canonical immunoglobulins (HCAb) are being extensively developed. These antibodies do not contain the light chain. HCAbs were first discovered in dromedary [4]. Later it was shown that HCAbs, as well as classical antibodies, are present in the blood of cartilaginous fish and mammals of the *Camelidae* family. HCAbs were also found in the blood of humans exposed to gamma radiation, though, in this case, they were non-functional.

The overall configuration of variable domains is similar in a classical antibody (V_H domain) and noncanonical one (V_HH domain). Three variable regions (complementarity determining regions,

CDRs) often stabilized by disulfide bonds are located in loops between two β-sheets. Variable regions in the V_HH domain are longer than those in canonical antibodies [5], they form extended loops. This enables HCAbs to recognize epitopes with a concave surface (for instance, active centers of enzymes) [6], which are often inaccessible to classical antibodies. HCAbs also feature other useful properties, including reduced immunogenicity, increased solubility, and high thermal and pH stability, and they easily penetrate into various tissues. In spite of their high potential and unique specificity compared to classical IgG, using V_HH domains (also named single-domain antibodies or nanobodies) in the therapy of various diseases is limited due to rapid plasma clearance [7–9]. There are two basic approaches to extend the half-life of recombinant single-domain antibodies in the plasma: increasing the hydrodynamic radius of the molecule (conjugation with PEG and other polymers), obtaining a V_HH linked to the Fc fragment [10], modification of the Fc regions of antibodies and conjugation with albumin [11]. Success was also achieved in a strategy of nanoantibody dimerization. In this case, one antibody was directed against an antigen while the other one against albumin [12].

Designing a Fab fragment of the classical antibody in which the V_HH domain is substituted for the V_H domain, is yet another promising solution [13,14]. In this work, we present the crystal structure of the netakimab Fab fragment, which is directed against the IL-17A, kinetic analysis of the interaction between IL-17A with the Fab fragment and its integral part, the V_HH domain, and modeling the interactions in the IL-17A/V_HH domain complex.

Netakimab is a humanized monoclonal anti-IL-17 antibody that belongs to the IgG1/κ type. The light chain belongs to the VK3 structural family and contains domains CL and VL. The heavy chain consists of constant domains CH3, CH2, and CH1; the variable domain V_H is substituted with a variable domain of a non-canonical antibody, V_HH. The netakimab Fab fragment demonstrates functional activity, which is higher than that of the widely applied therapeutic preparation secukinumab.

Presently, netakimab in a highly concentrated subcutaneous form is being tested in a phase III clinical trial (Identifier NCT03390101 for ClinicalTrials.gov) in patients with moderate to severe vulgar psoriasis. The netakimab preparation demonstrates high efficiency (over 90% of patients reached PASI (Psoriasis Area and Severity Index) 75 at week 12), high solubility (up to 60 mg/mL), and a high safety profile [15], which indicates its physicochemical and biological stability upon therapeutic application. We suggested that tighter contact between the V_HH domain of the netakimab Fab fragment and the IL-17A region that interact with the IL-17 RA receptor provides high functional activity of the preparation.

2. Materials and Methods

2.1. Production and Purification of the Fab Fragment and IL-17A

For transient expression of the gene for the netakimab Fab fragment (the Fab fragment), Chinese hamster ovary CHO-K1-S line at a density of 2×10^6 cells/mL was transfected with a pTT-5-BCD-085-Fab plasmid, which carries genes of light and heavy chains of the Fab fragment, in the presence of polyethyleneimine (PEI, Polysciences, Inc., Warrington, PA, USA). DNA/PEI ratio was 1:3 to 1:10. Cells were cultured in the FreeStyle CHO (GIBCO) in a suspension in flasks in a shaker-incubator (Multitron) for seven days. Cultures were centrifuged at 2000× *g* for 20 min and filtered through a 0.22 μm filter (Millipore).

The recombinant Fab fragment, which contained a hexa-histidine tag at the C-terminus of the heavy chain, was purified from the culture medium using Profinity IMAC Ni-charged resin (Bio-Rad). Culture medium was successively supplemented with $NiCl_2$ to a concentration of 1 mM and 5 mL of the resin, mixed in a shaker for one hour at room temperature. The resin was then transferred to a 5 mL column (Thermo Scientific), washed with five column volumes of PBS. The Fab fragment was eluted with a buffer A (300 mM imidazole, 150 mM NaCl, Na-phosphate buffer pH 8.0). Fractions containing the purified protein were concentrated and dialyzed against a buffer B (150 mM NaCl, 50 mM sodium acetate, pH 5.5). The obtained preparation was further purified using the size exclusion

chromatography on the Superdex G-75 resin (GE Healthcare) equilibrated in buffer B (Supplementary Figure S1A). At every step of purification, protein preparations were controlled by gel electrophoresis under denaturing conditions.

2.2. Production and Purification of the V_HH Domain

Gene of the single-domain anti-IL-17A antibody (V_HH domain) was (PCR-amplified using primers V_HH_For, 5′-GCTGGAATTCGAAGTTCAACTGGTGCAG-3′, and V_HH_Rev, 5′-CAGGGGAAGCTTTTATGAGGAGACGGTGACCAG-3′ and pTT-5-V_HH anti-IL-17A plasmid as a template) cloned in the pET-28a vector between *Eco*RI and *Hind*III cloning sites. The obtained genetic construction was validated by sequencing and used for transformation of the *Escherichia coli* strain BL21(DE3)/Rosetta. The transformants were grown in a liquid LB medium supplemented with kanamycin (50 μg/mL) and chloramphenicol (25 μg/mL) at 310 K with rotation (150 revolutions per minute). Synthesis of the V_HH domain was induced at A_{260} = 0.6 by adding IPTG (0.3 mM) and cultures were grown for another three hours under the same conditions. Cells were harvested by the centrifugation at 8000× *g* for 15 min.

The obtained cell mass was suspended in buffer C (500 mM NaCl, 50 mM Tris-HCl, pH 7.0, 10 mM imidazole). Cells were disrupted by sonication at 277 K. Cell debris was removed by the centrifugation at 15,000× *g* for 30 min at 277 K. The supernatant was loaded onto a Ni-NTA agarose (GE Healthcare) column equilibrated with buffer C. The V_HH domain was eluted using a step gradient of imidazole concentration (20 mM, 40 mM, and 150 mM) in buffer C. Fractions containing the protein were concentrated and dialyzed against buffer B. The obtained preparation was further purified by the size exclusion chromatography on the Superdex G-75 resin equilibrated with buffer B (Supplementary Figure S1B). At every stage, preparations were analyzed by gel electrophoresis under denaturing conditions.

2.3. Circular Dichroism Measurements

CD measurements were performed on a Chirascan Spectrometer (Applied Photophysics, UK) equipped with a Julabo F25 computer-controlled thermostat. Spectra were registered using cuvettes with 0.1 mm path length. CD spectra of V_HH are typical for that of an ordered globular protein (Supplementary Figure S2).

2.4. Production and Purification of IL-17A

The human IL-17A gene was overexpressed using the method identical to that for obtaining the Fab fragment. The pTT-5-IL-17A plasmid carrying genes of intact human IL-17A was used. Purification of IL-17A from culture liquid was performed using the Profinity IMAC Ni-charged (Bio-Rad) resin as described for the purification of the Fab fragment. Fractions containing pure protein were concentrated and dialyzed against buffer B.

2.5. Analysis of the Interaction of the Fab Fragment and the V_HH domain with IL-17A by Surface Plasmon Resonance Approach (SPR)

Measurements were carried out using OCTET RED96 apparatus (Pall Forte Bio) in a running buffer (PBS supplemented with 0.1% BSA and 0.1% Tween-20) at 303 K. Biosensors AR2G (Pall Forte Bio) were rehydrated for one hour in deionized water and activated in 20 mM 1-Ethyl-3-(3-dimethylaminopropyl) carbodiimide hydrochloride (EDC)/10 mM N-hydroxy(sulfo) succinimide (Sulfo-NHS). IL-17A at a concentration of 25 μg/mL in 10 mM sodium acetate (pH 4.0) was nonspecifically (through the amino groups) immobilized on the surface of the biosensor. After the neutralization with 1 M Ethanolamine (pH 8.5), sensors were immersed into in wells containing solutions of the Fab fragment at concentrations ranging from 2.5 nM to 20 nM or with V_HH domain solutions at concentrations ranging from 1.25 nM to 10 nM. Sensors were then immersed into the running buffer for the subsequent dissociation stage; duration of association stage was 1000 s, and the dissociation stage was 3600 s. The curves obtained

were analyzed using the Octet System Data Analysis software and 1:1 Langmuir binding model. The measurements were repeated 3 times.

2.6. Crystallization of the Fab Fragment

Crystallization experiments were performed at 298 K using the hanging-drop vapor-diffusion method on siliconized glass cover slides in Linbro plates. Drops were made by mixing a protein solution at 20 mg/mL in 50 mM sodium acetate pH 5.5, 150 mM NaCl with a well solution—1.5 M $(NH_4)_2SO_4$, 150 mM sodium citrate pH 5.5 (condition No. 15 of Stura FootPrint Screen I from Molecular Dimensions) at 1:1 volume ratio. Crystals appeared in 20 days and grew to maximum dimensions of 0.2 mm × 0.05 mm × 0.2 mm. Before freezing in liquid nitrogen, the crystals were transferred to a solution composed of 1.6 M $(NH_4)_2SO_4$, 20% glycerol, 80 mM sodium acetate trihydrate pH 4.6.

2.7. Diffraction Data Collection and Determining the Structure of the Fab Fragment

Diffraction data were collected to 1.9 Å resolution on the ID23-1 beamline at the European Synchrotron Radiation Facility (ESRF), Grenoble, France [16] equipped with a Pilatus 6M detector. Data collection was controlled by the MxCuBE system [17] and the strategy was calculated by BEST [18]. Data were processed and scaled with the XDS package [19]. The crystals of the Fab fragment BCD-085 belonged to space group $P2_12_12_1$ with unit cell parameters a = 90.56, b = 111.92, c = 165.43 Å, and four heterodimer molecules in the asymmetric unit.

The structure was solved by molecular replacement with Phaser [20] using the structure of the light chain from the crystal structure of human germline antibody IGHV5-51/IGKV3-20 (PDB entry 5I1K) and for the heavy chain structure of the broadly neutralizing human anti-hepatitis C virus (HCV) glycoprotein E2 Fab fragment HC33.4 (PDB entry 5FGB) as a search model. Water molecules and metal ions were removed from the model. The initial model was subjected to crystallographic refinement with REFMAC5 [21]. Manual rebuilding of the model was carried out in Coot [22]. The final model of the Fab fragment, refined to an R factor of 16.8% and Rfree of 22.8% at 1.9 Å resolution. Data and refinement statistics are summarized in Table 1. The coordinates and structure factors have been deposited in the Protein Data Bank (PDB entry 6QKD). Figures were prepared using PyMOL [23].

Table 1. Data collection and refinement statistics.

Data Collection	
Wavelength (Å)	0.97242
Space group	$P2_12_12_1$ (No. 19)
Unit-cell parameters (Å, °)	*a* = 90.56, *b* = 111.92, c = 165.43, α = γ =β = 90
Resolution limits (Å)	50.0–1.9 (2.01–1.9)
Completeness (%)	99.7 (98.7)
Measured reflections	815,153 (124,199)
Unique reflections	132,510 (20,959)
R_{merge} (%)	5.3 (99.8)
Mean I/σ (I)	19.2 (1.7)
Redundancy	6.2 (5.9)
CC(1/2)	100.0 (88.6)
Refinement	
Resolution (Å)	47.6–1.9 (1.95–1.9)
No. of reflections	125,855 (8961)
R factor (%)	16.8 (31.8)
Free R factor (%)	22.8 (37.6)

Table 1. *Cont.*

Refinement	
Average overall B factor (^{2})	48.8
Ramachandran plot	
Most favored (%)	97.3
Allowed (%)	2.7
R.m.s. deviations	
Bond lengths (Å)	0.010
Bond angles (°)	1.291
PDB code	6QKD

Data were collected at 100 K. Values in parentheses are for the last resolution shell.

2.8. Docking and Molecular Dynamics Simulations

For complex modeling, we use a combination of information from IL-17A/ IL-17A RA complex and best structures constructed from V_HH and IL-17A dimer by docking at HDOCK web server [24]. The molecular dynamics simulations of the V_HH domain and IL-17A complex were performed using the Gromacs 4.5.3 program [25] with Charmm27 all-atom force fields [26,27]. The lengths of covalent bonds involving hydrogen atoms were constrained using the LINCS algorithm [28], which enabled us to use the integration step of 2fs. Electrostatic interactions were estimated using the particle mesh Ewald (PME) technique [29,30]. Van der Waals interactions were described using the switch functions in the range of 10–12 Å. A constant temperature (300 K) was maintained with the velocity rescale (v-rescale) thermostat [25]. The Berendsen barostat was applied to maintain the pressure of the system at 1 atm [31].

The molecular dynamics simulations were performed using the three-dimensional structure of the V_HH domain of the Fab fragment in a complex with IL-17A as the starting model. To check the quality of the parameters used in the calculations, the stereochemical parameters of the models obtained after 2ns molecular dynamics simulations were compared with the experimental structures of the corresponding molecules. Three 200ns molecular dynamics trajectories were calculated at a constant temperature of 300 K and a pressure of 1 atm. All molecular dynamics trajectories were calculated using resources of the Joint Supercomputer Center of the Russian Academy of Sciences (JSCC RAS, www.jscc.ru). The PISA (protein interfaces, surfaces, and assemblies) service at the European Bioinformatics Institute [32] was used for calculating contact areas and bond lengths [33].

3. Results

3.1. Crystal Structure of the Fab Fragment of Netakimab at 1.9 Å Resolution

The asymmetric unit contains four netakimab Fab fragment molecules. C-terminal (constant) domains of heavy and light chains interact with each other in a classic way, whereas N-terminal ones do not, only small contacts with neighboring heterodimer molecules are observed. (Figure 1A, and Figure 2A). Therefore, the netakimab Fab fragment molecule acquires a V-shaped form, which differs from the form of classical Fab fragments (Figure 1B). High diversity in conformations of loops in the four netakimab Fab fragment molecules is observed that causes variations in the regions of interactions between nearby molecules. We suggested that these interactions between constant domains of heavy and light chains in the asymmetric unit do not have an impact on the functional properties of the netakimab Fab fragment. Protein–protein contacts between the antibody variable domains of heavy and light chains, as well as contacts between variable domains of heavy and light chains in different molecules in the asymmetric unit vary considerably. Therefore, these chains are located at different angles and on different distances in the asymmetric unit (Figure 2A). The angle between extreme positions of heavy chain domains is about 32°, whereas the angle between the extreme positions of the

light chains is about 18° (Figure 2B). Such variability in orientations of light and heavy chains of the Fab fragment within the crystal unit suggests high levels of mobility.

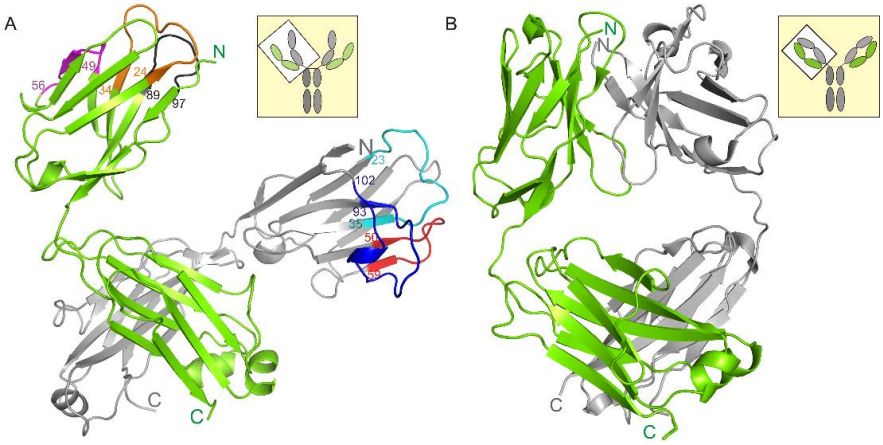

Figure 1. The structure of the netakimab Fab fragment. (**A**) The netakimab Fab fragment, light chain is colored green, heavy chain–gray. CDR-H1–cyan, CDR-H2–red, CDR-H3–blue. CDR-L1–brown, CDR-L2–violet, CDR-L3–black. Position numbers are shown for amino acid residues at the beginning and the end of CDRs. (**B**) The crystal structure of the human germline antibody IGHV5-51/IGKV3-20 (PDB entry 5I1K), light chain–green, heavy chain–gray.

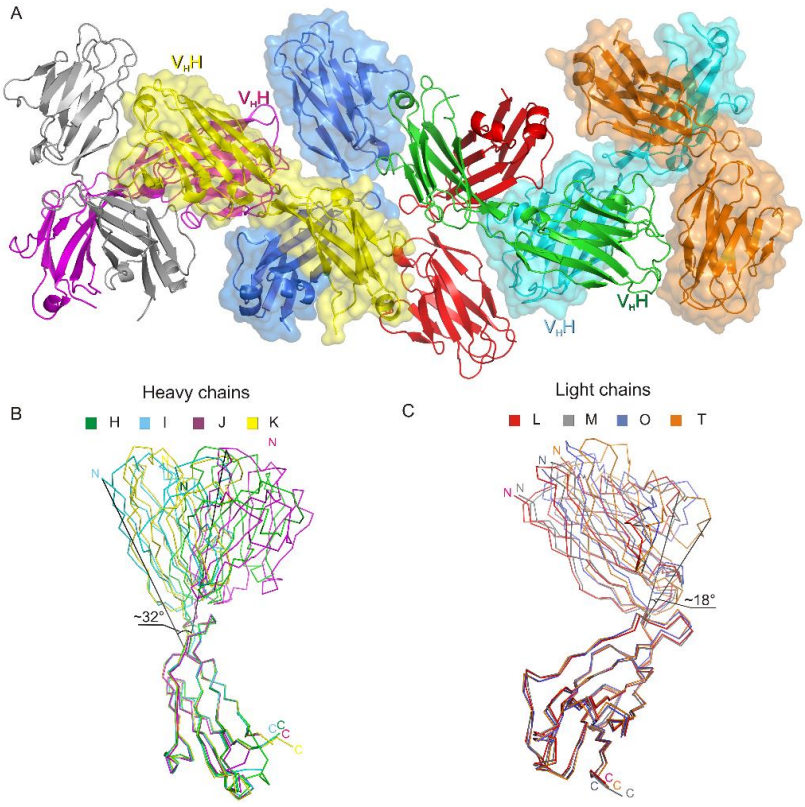

Figure 2. The crystal packing of the netakimab Fab fragment. (**A**) Crystal packing of the four Fab fragment molecules in the asymmetric unit. Heavy and light chains are indicated with different colors, surfaces of even molecules are colored. (**B**) Structural alignment of the different conformations obtained for the heavy chains (H, I, J, K). (**C**) Structural alignment of the different conformations obtained for the light chains. Extreme fluctuation angles for variable domains relatively to constant domains are indicated (the angle vertices are at the last matching Cα atoms of the main chains).

3.2. Kinetic Analysis

The affinity of the V_HH domain and the V_HH-based Fab fragment for IL-17A was assessed using SPR (Figure 3). Kinetic constants and equilibrium dissociation constants (K_D) of complexes of the Fab fragment and the V_HH domain with IL-17A were determined using global fitting of the four curves and 1:1 Langmuir interaction model (Table 2). Kinetic analysis of binding the Fab fragment with IL-17A and results of gel-filtration chromatography (not shown) evidences that the Fab fragment forms a stable complex with the IL-17A dimer at a molar ratio of 1:1.

Table 2. Kinetic Constants of Interactions of IL-17A with the Fab Fragment and the V_HH Domain.

Protein	k_a (M^{-1} s^{-1})	k_d (s^{-1})	K_D (nM)
Fab fragment	6.3×10^4	2.0×10^{-5}	0.3
V_HH domain	5.0×10^5	4.3×10^{-5}	0.09

As we did not succeed in obtaining crystals of V_HH alone or with IL-17A or complexed with IL-17A suitable for the X-ray analysis, we simulated the interactions between the IL-17A dimer and the V_HH domain as a part of the Fab fragment.

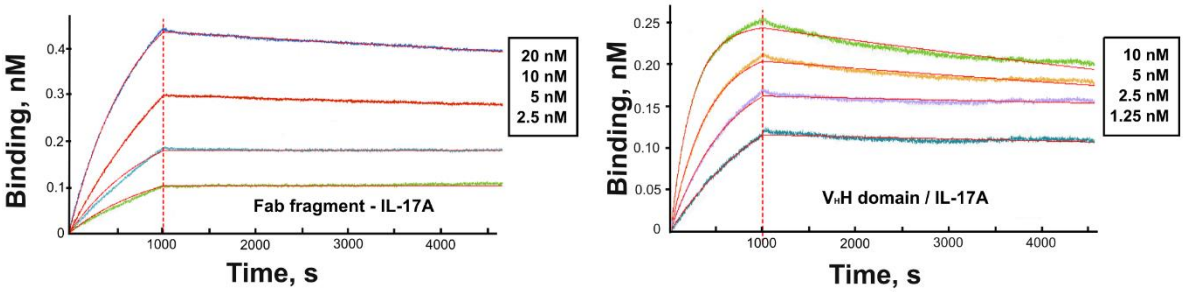

Figure 3. Sensograms of the interaction of the V_HH domain (alone or as a part of the Fab fragment) with IL-17A. The experimental curves are shown in different colors while fitted curves are in red.

3.3. Modeling the V_HH Domain/IL-17A Complex

As reliable modeling interactions between the entire Fab fragment and IL-17A do not seem to be possible due to high conformational plasticity of the molecule, we performed modeling of the V_HH domain as a part of the Fab fragment with the IL-17A dimer. IL-17A model was used from the structure of the IL-17A/ IL-17A RA complex (PDB entry 4HSA), as it is currently the most complete IL-17A model, in which the N-terminal region including the β_0 strand and flexible loop between β_0 and main β sheet stabilized by IL-17A RA [34]. Possible intermolecular hydrogen bonds and hydrophobic interactions upon the complex formation were determined.

4. Discussion

A fraction of functional antibodies in *Camelidae* lacks light chains. Their variable domains represent single-domain antibodies with a molecular weight of 15 kDa. Due to their small size, the nanoantibodies are rapidly excreted from the organism by the kidneys. In general, the half-life of nanoantibodies in human blood does not exceed 2 hours, which is significantly shorter than the half-life of classical monoclonal antibodies [35]. Therefore, design and medical application of chimeric antibodies containing V_HH domains is highly relevant. However, the structure of such chimeric Fab fragments has not yet been determined. We have determined the structure of the netakimab Fab fragment containing the anti-IL17A V_HH domain and performed modeling of the interaction between the anti-IL-17A V_HH domain and IL-17A.

4.1. Structure of the Netakimab Fab Fragment

CDR loops of the Fab fragment light and heavy chains that link structural elements of β-sheets were classified according to the work [36] based on their belonging to canonical clusters (Table 3). This classification is similar to the one published by Martin and coworkers [37], but CDR-H1 and CDR-H3 begin right after cysteine residues and CDR-L2 includes Tyr at the N-terminal part.

Table 3. Comparison of H- and L-loops of the netakimab Fab fragment with the canonical types (clustering according to [36]).

Region Name	Residues (Kabat Database)	Cluster (Length)	Median PDB Entry
HFR1	1-22		
CDR-H1	23-35	H1-13-3 (13 aa)	1U0Q
HFR2	36-49		
CDR-H2	50-58	H2-10-2 (10 aa)	1SEQ
HFR3	59-92		
CDR-H3	93-102	18 aa	1MVF
HFR4	103-113		
LFR1	1-23		
CDR-L1	24-34	L1-12-2 (12 aa)	2FX7
LFR2	35-48		
CDR-L2	49-56	L2-8-5 (8 aa)	1IGM
LFR3	57-88		
CDR-L3	89-97	L3-9cis7-1 (9 aa)	1IGM
LFR4	98-109		

CDR regions of the netakimab Fab fragment variable domains of light chains have conformations similar to that of canonical type clusters (Table 3, Figure 4). Variable domains of the netakimab Fab fragment heavy chains demonstrate lower (as compared to corresponding domains of light chains) structural similarity to the canonical structures.

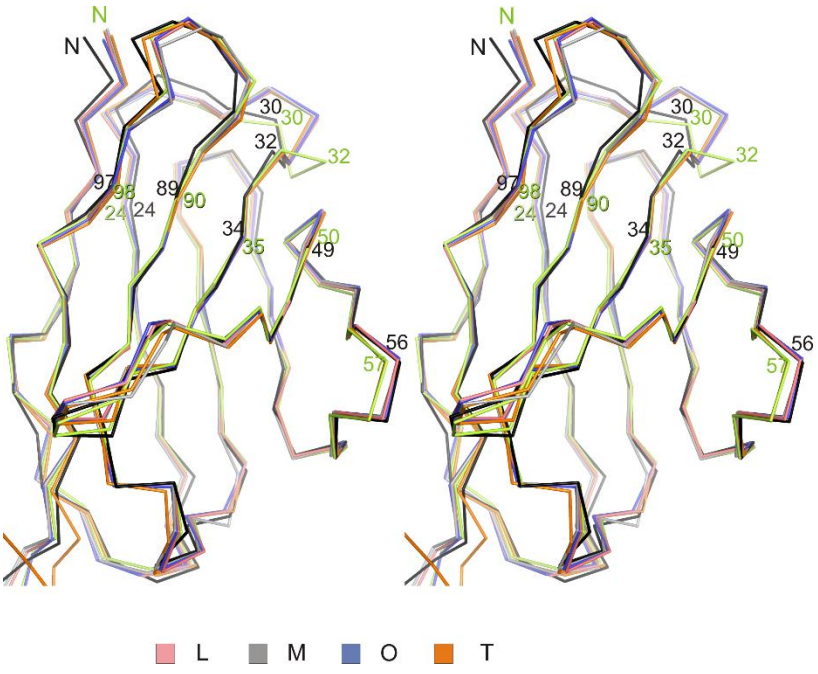

Figure 4. Structural alignment of variable domains of light chains. A stereo view of structural alignment of Cα chains of variable domains of the four netakimab Fab molecules (L,M,O,T) and corresponding regions of light chains of antibodies, whose structures have similar structural organization of the CDR regions (green: human germline antibody IGHV5-51/IGKV3-20; black: FV from human IGM immunoglobulin).

We have shown that the CDR-H1 (13 amino acids long) of the Fab fragment (Figure 5A) belongs to the H1-13-3 cluster (the most similar structure is PDB entry 1SEQ). In the region between residues 24 and 31, there is relatively high chain mobility in different molecules in an asymmetrical unit. However, the main chain conformation in molecules in a crystallographic unit is preserved. CDR-H2 (10 amino acids long) belongs to the H2-10-2 cluster (Table 3, Figure 5B), differences from the most similar structure are only marginal. It is worth mentioning that there are differences in the structure of the loop (70-79 aa), which belongs to the framework part of HFR3 (Figure 5C).

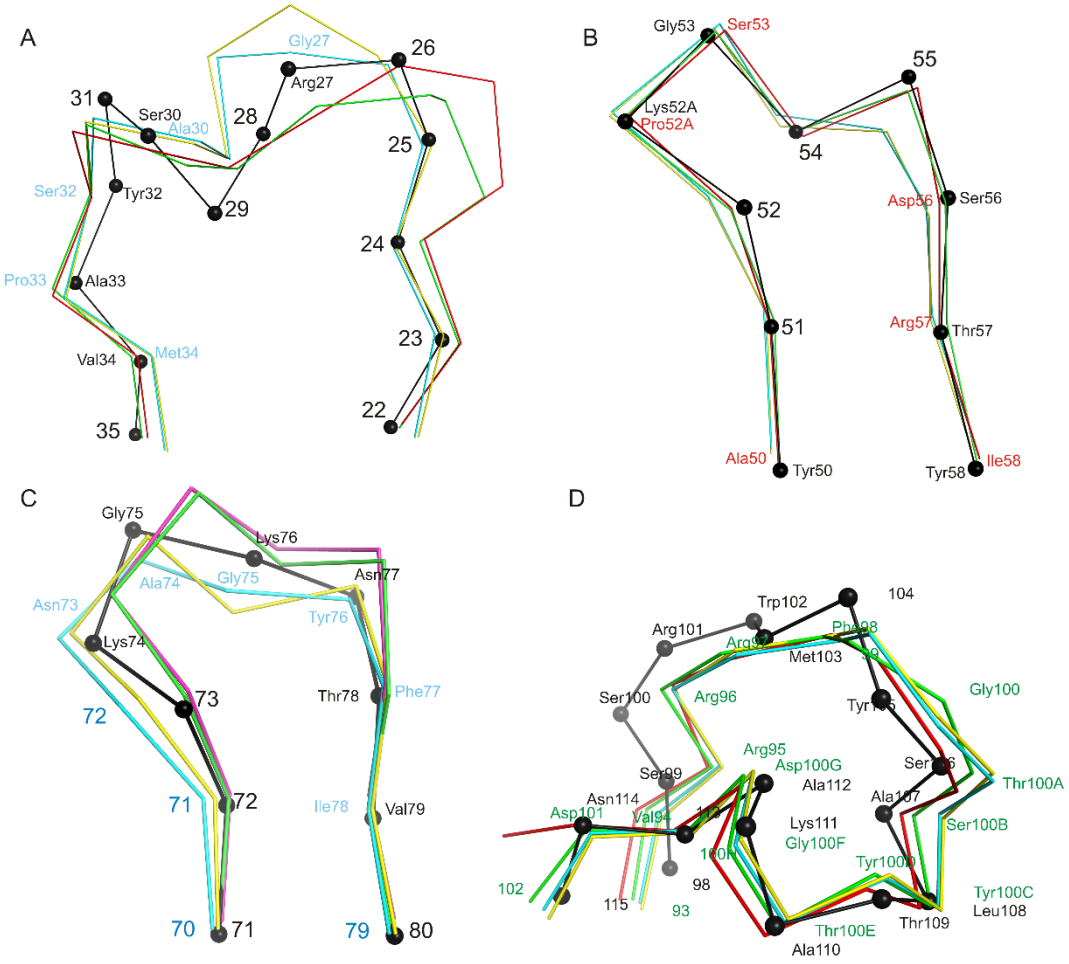

Figure 5. Structural alignment of CDR loops of heavy chains and HFR3. Structural alignment of Cα atoms of CDR loops of heavy chains and HFR3 of four netakimab Fab fragment molecules and Cα atoms (black) of the most similar structures listed in Table 3 (for CDR loops) and PDB entry 2P45 (for HFR3). Cα atoms of the Fab fragment are colored variously. If amino acids coincide, only position number is provided, whereas both name and position are indicated if they differ. (**A**) CDR-H1, (**B**) CDR-H2, (**C**) HFR3, (**D**) CDR-H3.

The netakimab Fab fragment CDR-H3 loop is relatively long (18 residues between positions 94 and 102 according to Kabat Database). Unusual V-shaped conformation of the Fab fragment molecule is determined by the specificity of the CDR-H3 V_HH domain sequence. Elongated CDR-H3 region forming "beak" causes a change of the surface (V_L side) of the V_HH domain within the Fab fragment, which prevents its interaction with the V_L chain. In addition to aromatic residues (three tyrosines and one phenylalanine), the CDR-H3 loop features high content of charged residues: three arginines and three aspartates. CDR-H3 structure is stabilized by at least ten hydrogen bonds (Figure 6). Interaction of CDR-H3 with the V_HH domain is realized by means of hydrophobic interactions of the loop residues

Tyr100C, Thr100E and Tyr100H with Gly35, Leu37, and Phe47 belonging to HFR2, and with Ala50 and Ile58 located at the beginning and at the end of CDR-H2.

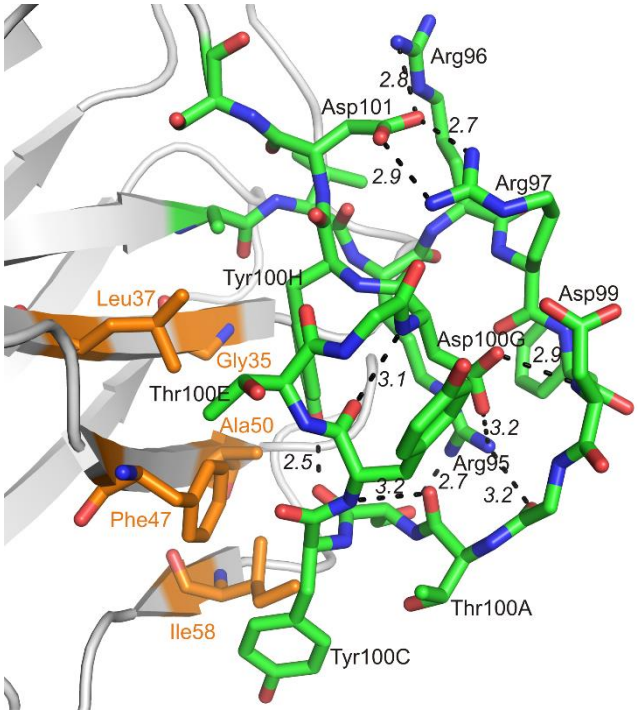

Figure 6. Interaction within the CDR-H3 loop (green) and its contacts with amino acid residues of the V_HH domain as part of the Fab fragment (orange).

High variability in the orientation of light and heavy chains of the netakimab Fab fragment in the asymmetric unit may indicate their high mobility in vivo. Comparative analysis of structures of Fab antibody fragments from the PDB reveals high interdomain mobility in molecules of various Fab fragments alone [38] and complexed [39]. In our case, there is a high range of Fab conformations between the constant and variable domains in a single crystal structure.

4.2. Modeling the V_HH Domain/IL-17A Complex

As the position of variable domains of light and heavy chains of the netakimab Fab fragment molecules varies in the asymmetric unit (Figure 2), modeling its complex with IL-17A is complicated. Therefore, to assess interactions of the cytokine with the netakimab Fab fragment, we used a part of the structure containing the V_HH domain. The affinity of the V_HH domain to IL-17A (K_D = 0.09 nM) is comparable to that of the netakimab Fab fragment for the cytokine (K_D = 0.3 nM) (Table 2), which suggests that protein-protein contacts in the V_HH/IL-17A complex are decisive for the Fab fragment binding to IL-17A. The functional activity of the V_HH domain (the ability to inhibit production of interleukin 6 in the cell line HT1080 [ATCC:CCL-121]) is also preserved in the structure of the Fab fragment (Table 4).

Table 4. Anti-IL-17A antibodies. K_D for antibody-cytokine complexes and half-maximal inhibitory concentrations.

Anti-IL-17A antibody	K_D (nM)	IC_{50} (pM)	Reference
netakimab Fab fragment	0.3	66	this article and [41]
V_HH domain	0.09	30	this article and [13]
Secukinumab	0.12	201	[42]
CAT 2200 Fab fragment	2.1	1560	[40]

Currently, the V_HH/IL-17A complex is one of the most stable complexes of this cytokine. Antigen affinity for the IL-17RA receptor [34] and the Fab fragment of the CAT 2200 antibody [40] is one order of magnitude lower (K_D = 0.3 and 2.1 nM, respectively, Table 4). Modeling the V_HH/IL-17A complex allowed suggesting reasons for such strong binding.

For modeling the V_HH/IL-17A complex we used the IL-17A structure from its complex with the receptor, as it is the most complete one. It is known that IL-17A forms a functional dimer (monomers A and B). Mobile N-terminal part of IL-17A is virtually invisible in the electron density maps of both individual molecule and bound to the CAT 2200 Fab fragment. However, in a complex with the IL-17RA receptor the N-terminal part of one of the IL-17A monomers is clearly visible.

The molecule of the V_HH domain is capable of forming a complex with both IL-17A monomers forming eleven hydrogen bonds and five hydrophobic contacts (Table 5).

Table 5. V_HH domain/IL-17A direct interactions. The residue position includes a chain indicator (H: V_HH domain; A: IL-17A monomer A; B: IL-17A monomer B). The distance cutoff used for hydrogen bonds is 3.5 Å, and for nonpolar interactions is 5.0 Å.

V_HH Domain	Distance (Å)	IL-17A
Hydrogen bonds		
Gly H42 O	3.27	Gln A94 NE2
Lys H43 NZ	2.92	Glu A95 OE2
Glu H85 OE1	2.66	Lys B38 NZ
Arg H97 NH2	3.09	Pro B59 O
Asp H99 OD1	2.58	Arg B101 NH2
Asp H99 OD2	3.19	Asn B108 ND2
Thr H100A OG1	3.55	Asn A17 ND2
Gly H100F O	2.90	Arg B101 NH1
Asp H100G OD1	2.73	Arg B101 NH2
Ser H102 OG	2.69	Glu B57 OE2
Ser H102 OG	3.01	Arg B55 NH1
Nonpolar (distance corresponds to the closest atom pair)		
Thr H100A CG2	3.70	Ile B28 CD
Thr H100A CG2	4.63	Leu B26 CG
Tyr H100C CB	3.56	Ile B28 CD
Tyr H100D CE1	3.53	Tyr B62 CD2
Tyr H100D CZ	3.88	Phe B110 CZ

A region of the V_HH domain due to a specific spatial organization of CDR-H3 (Figure 7), penetrates a hollow on the IL-17A surface forming multiple contacts. The IL-17A monomer A in the model of the complex forms three hydrogen bonds with the V_HH domain (two with HFR2 and one with CDR-H3), whereas monomer B forms eight hydrogen bonds and five hydrophobic contacts, most of which are also located in CDR-H3. The surface of the intermolecular contact in the V_HH/IL-17A complex may be divided into two regions (Figure 7), which correspond to two out of three regions of IL-17A interaction with the IL-17 RA receptor. Region 1 is formed by the N-terminal part of IL-17A, region 2 is formed by the central part of β-sheets of the dimer. We suggest that as the N-terminal part of IL-17A is essential for binding with IL-17A RA it could participate in binding with the V_HH domain (hydrogen bind Lys38-Glu85, Table 5).

Using the PISA service we compared contact areas in our V_HH/IL-17A complex and a complex between IL-17A and the CAT 2200 antibody Fab fragment (PDB entry 2VXS) (Supplementary Figure S3B). Total contact area in the V_HH/IL-17A complex was 1185 Å^2 (963 Å^2 with monomer B and 222 Å^2 with monomer A). The contact area in the complex with the CAT 2200 antibody included seven hydrogen bonds and it was less extensive–833 Å^2. However, most of the interactions were also recorded for monomer B (607 Å^2). Moreover, interactions occurred with both heavy and light chains of the Fab fragment. Superposition of the structure of the netakimab Fab fragment and the structure of V_HH in the model complex (Supplementary Figure S3A) did not show significant clashes of the

light chain of the Fab fragment with the dimer IL-17A. Thus, comparative structural analysis of the IL-17A complexes can explain the increased the V_HH domain affinity for IL-17A by enlarged area of protein-protein contacts due to additional interactions between CDR-H3 and the cytokine dimer.

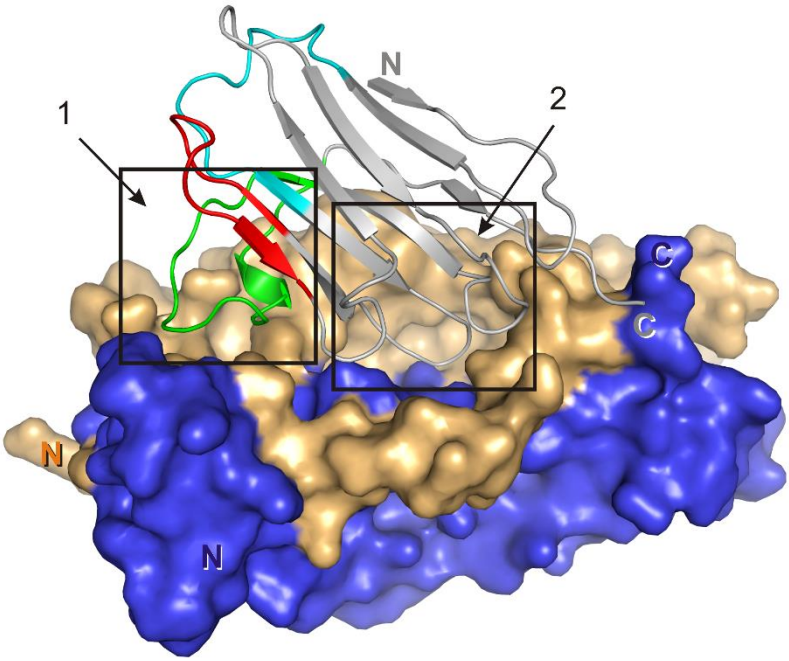

Figure 7. V_HH/IL-17A complex. Surface of the IL-17A dimer is shown (monomer A is dark blue, monomer B is yellow). Crystallographic model of the V_HH domain is in gray. CDR-H1–cyan, CDR-H2–red, CDR-H3–green. The two contacting regions are indicated by frames.

Correlation is observed between the antibody affinity for the cytokine and its functional activity (Table 4). The V_HH domain demonstrates full functional activity, which is 6.6-fold higher than that of the widely applied therapeutic preparation secukinumab. Presumably, tighter contact between the V_HH domain and the IL-17A region that interact with the IL-17 RA receptor provides the high functional activity of the preparation. Thus, the netakimab Fab fragment carrying the V_HH domain may become the most efficient therapeutic preparation for treating psoriasis, and the structural data obtained can be used for the further design of effective cytokine inhibitors.

Supplementary Materials: The following are available online at http://www.mdpi.com/2073-4352/9/3/177/s1, Figure S1: Elution profiles of size-exclusion chromatography and SDS–PAGE gel of purified Fab (A) and V_HH domain (B). Lane M – molecular-weight marker, Figure S2: Circular dichroism spectrum of V_HH domain, Figure S3: (A) Netakimab Fab fragment /IL-17A complex. Surface of the IL-17A dimer is shown (monomer A is dark blue, monomer B is yellow). Crystal structure of Fab fragment (light chain is colored green, heavy chain–gray). (B) Fab fragment CAT 2200/ IL-17A complex (PDB ID 2VXS). Monomer A of IL-17A is dark blue, monomer B is yellow. Light chain Fab fragment CAT 2200 of is colored green, heavy chain–gray.

Author Contributions: Conceptualization: O.K., M.G., data curation: O.K., A.G., formal analysis: A.G., funding acquisition: O.K., A.G., investigation: S.E., A.U., methodology: O.K., I.K., V.E., S.E., A.G., project administration: S.T., M.G., resources: I.K., V.E., supervision: O.K., S.T., validation: A.U., O.K., visualization: A.G., S.E., writing: O.K., S.T., A.G. wrote the paper with input from all authors.

Funding: This work was supported by the Russian Science Foundation (grant number 177410156).

Acknowledgments: We acknowledge the Structural Biology Group of the European Synchrotron Radiation Facility for granting access to the synchrotron beamlines.

Conflicts of Interest: The authors declare no conflict of interest.

References

1. Cypowyj, S.; Picard, C.; Maródi, L.; Casanova, J.-L.; Puel, A. Immunity to Infection in IL-17-Deficient Mice and Humans. *Eur. J. Immunol.* **2012**, *42*, 2246–2254. [CrossRef]
2. Beringer, A.; Noack, M.; Miossec, P. IL-17 in Chronic Inflammation: From Discovery to Targeting. *Trends Mol. Med.* **2016**, *22*, 230–241. [CrossRef]
3. Paek, S.Y.; Frieder, J.; Kivelevitch, D.; Menter, M.A. IL-17 Inhibitors for Psoriasis. *Semin. Cutan. Med. Surg.* **2018**, *37*, 148–157. [CrossRef]
4. Wolfson, W. Ablynx Makes Nanobodies from Llama Bodies. *Chem. Biol.* **2006**, *13*, 1243–1244. [CrossRef] [PubMed]
5. Muyldermans, S. Single domain camel antibodies: Current status. *J. Biotechnol.* **2001**, *74*, 277–302. [CrossRef]
6. Schmitz, K.R.; Bagchi, A.; Roovers, R.C.; van Bergen en Henegouwen, P.M.P.; Ferguson, K.M. Structural Evaluation of EGFR Inhibition Mechanisms for nanobodies/VHH Domains. *Structure* **2013**, *21*, 1214–1224. [CrossRef]
7. Cortez-Retamozo, V. Efficient Cancer Therapy with a Nanobody-Based Conjugate. *Cancer Res.* **2004**, *64*, 2853–2857. [CrossRef]
8. Cortez-Retamozo, V.; Lauwereys, M.; Hassanzadeh, G.; Gobert, M.; Conrath, K.; Muyldermans, S.; De Baetselier, P.; Revets, H. Efficient Tumor Targeting by Single-Domain Antibody Fragments of Camels. *Int. J. Cancer* **2002**, *98*, 456–462. [CrossRef]
9. Harmsen, M.M.; Van Solt, C.B.; Fijten, H.P.D.; Van Setten, M.C. Prolonged in Vivo Residence Times of Llama Single-Domain Antibody Fragments in Pigs by Binding to Porcine Immunoglobulins. *Vaccine* **2005**, *23*, 4926–4934. [CrossRef] [PubMed]
10. Richard, G.; Meyers, A.J.; McLean, M.D.; Arbabi-Ghahroudi, M.; MacKenzie, R.; Hall, J.C. In Vivo Neutralization of α-Cobratoxin with High-Affinity Llama Single-Domain Antibodies (VHHs) and a VHH-Fc Antibody. *PLoS ONE* **2013**, *8*, e69495. [CrossRef] [PubMed]
11. Kontermann, R.E. Strategies to Extend Plasma Half-Lives of Recombinant Antibodies. *BioDrugs* **2009**, *23*, 93–109. [CrossRef] [PubMed]
12. Hoefman, S.; Ottevaere, I.; Baumeister, J.; Sargentini-Maier, M. Pre-Clinical Intravenous Serum Pharmacokinetics of Albumin Binding and Non-Half-Life Extended Nanobodies®. *Antibodies* **2015**, *4*, 141–156. [CrossRef]
13. Ulitin, A.; Evdokimov, S.; Soloviev, V.; Chernyh, Y.; Goncharova, O.; Korzhavin, D.; Chernovskaya, T.; Nemankin, T.; Ivanov, R.; Morozov, D.; et al. High Affinity and Aggregatively Stable Antibodies on the Basis of Variable Domains vl and a Derivative vhh. U.S. Patent 2016048188A1, 31 March 2016.
14. International Nonproprietary Names for Pharmaceutical Substances (INN). INN: List 80; *WHO Drug Information*; WHO: Geneva, Switzerland, 2018; Volume 32, pp. 425–508.
15. Samtsov, A.V.; Khairutdinov, V.R.; Bakulev, A.L.; Kubanov, A.A.; Karamova, A.E.; Artem'eva, A.V.; Korotaeva, T.V. Efficacy and Safety of BCD-085, a Novel Interleukin-17 Inhibitor. Results of Phase II Clinical Trial in Patients with Moderate-to-Severe Plaque Psoriasis. *Vestn. Dermatol. Venerol.* **2017**, *5*, 52–63. [CrossRef]
16. Nurizzo, D.; Mairs, T.; Guijarro, M.; Rey, V.; Meyer, J.; Fajardo, P.; Chavanne, J.; Biasci, J.C.; McSweeney, S.; Mitchell, E. The ID23-1 Structural Biology Beamline at the ESRF. *J. Synchrotron Radiat.* **2006**, *13 Pt 3*, 227–238. [CrossRef]
17. Gabadinho, J.; Beteva, A.; Guijarro, M.; Rey-Bakaikoa, V.; Spruce, D.; Bowler, M.W.; Brockhauser, S.; Flot, D.; Gordon, E.J.; Hall, D.R.; et al. MxCuBE: A Synchrotron Beamline Control Environment Customized for Macromolecular Crystallography Experiments. *J. Synchrotron Radiat.* **2010**, *17*, 700–707. [CrossRef]
18. Bourenkov, G.P.; Popov, A.N. Optimization of Data Collection Taking Radiation Damage into Account. *Acta Crystallogr. D Biol. Crystallogr.* **2010**, *66 Pt 4*, 409–419. [CrossRef]
19. Kabsch, W. XDS. *Acta Crystallogr. D Biol. Crystallogr.* **2010**, *66 Pt 2*, 125–132. [CrossRef]
20. McCoy, A.J.; Grosse-Kunstleve, R.W.; Adams, P.D.; Winn, M.D.; Storoni, L.C.; Read, R.J. Phaser Crystallographic Software. *J. Appl. Crystallogr.* **2007**, *40 Pt 4*, 658–674. [CrossRef]
21. Murshudov, G.N.; Skubák, P.; Lebedev, A.A.; Pannu, N.S.; Steiner, R.A.; Nicholls, R.A.; Winn, M.D.; Long, F.; Vagin, A.A. REFMAC5 for the Refinement of Macromolecular Crystal Structures. *Acta Crystallogr. D Biol. Crystallogr.* **2011**, *67 Pt 4*, 355–367. [CrossRef]

22. Emsley, P.; Lohkamp, B.; Scott, W.G.; Cowtan, K. Features and Development of Coot. *Acta Crystallogr. D Biol. Crystallogr.* **2010**, *66 Pt 4*, 486–501. [CrossRef]
23. The PyMOL Molecular Graphics System. Available online: https://pymol.org/2/ (accessed on 1 March 2019).
24. Yan, Y.; Zhang, D.; Zhou, P.; Li, B.; Huang, S. HDOCK: A web server for protein—Protein and protein—DNA/RNA docking based on a hybrid strategy. *Nucleic Acids Res.* **2017**, *45*, 365–373. [CrossRef] [PubMed]
25. Hess, B.; Kutzner, C.; van der Spoel, D.; Lindahl, E. GROMACS 4: Algorithms for Highly Efficient, Load-Balanced, and Scalable Molecular Simulation. *J. Chem. Theory Comput.* **2008**, *4*, 435–447. [CrossRef] [PubMed]
26. MacKerell, A.D.; Bashford, D.; Bellott, M.; Dunbrack, R.L.; Evanseck, J.D.; Field, M.J.; Fischer, S.; Gao, J.; Guo, H.; Ha, S.; et al. All-Atom Empirical Potential for Molecular Modeling and Dynamics Studies of Proteins. *J. Phys. Chem. B* **1998**, *102*, 3586–3616. [CrossRef]
27. Mackerell, A.D., Jr.; Feig, M.; Brooks, C.L., 3rd. Extending the Treatment of Backbone Energetics in Protein Force Fields: Limitations of Gas-Phase Quantum Mechanics in Reproducing Protein Conformational Distributions in Molecular Dynamics Simulations. *J. Comput. Chem.* **2004**, *25*, 1400–1415. [CrossRef] [PubMed]
28. Hess, B.; Bekker, H.; Berendsen, H.; Johannes, G. LINCS: A linear constraint solver for molecular simulations. *J. Comput. Chem.* **1997**, *18*, 1463–1472. [CrossRef]
29. Darden, T.; York, D.; Pedersen, L. Particle Mesh Ewald: An N log(N) Method for Ewald Sums in Large Systems. *J. Chem. Phys.* **1993**, *98*, 10089–10092. [CrossRef]
30. Essmann, U.; Perera, L.; Berkowitz, M.L.; Darden, T.; Lee, H.; Pedersen, L.G. A Smooth Particle Mesh Ewald Method. *J. Chem. Phys.* **1995**, *103*, 8577–8593. [CrossRef]
31. Berendsen, H.J.C.; Postma, J.P.M.; van Gunsteren, W.F.; DiNola, A.; Haak, J.R. Molecular Dynamics with Coupling to an External Bath. *J. Chem. Phys.* **1984**, *81*, 3684–3690. [CrossRef]
32. PDBePISA (Proteins, Interfaces, Structures and Assemblies). Available online: http://www.ebi.ac.uk/pdbe/prot_int/pistart.html (accessed on 1 March 2019).
33. Krissinel, E.; Henrick, K. Inference of Macromolecular Assemblies from Crystalline State. *J. Mol. Biol.* **2007**, *372*, 774–797. [CrossRef]
34. Liu, S.; Song, X.; Chrunyk, B.A.; Shanker, S.; Hoth, L.R.; Marr, E.S.; Griffor, M.C. Crystal Structures of Interleukin 17A and Its Complex with IL-17 Receptor A. *Nat. Commun.* **2013**, *4*, 1888. [CrossRef]
35. Hassanzadeh-Ghassabeh, G.; Devooght, N.; Pauw, P.; Vincke, C.; Muyldermans, S. Nanobodies and their potential applications. *Nanomedicine* **2013**, *8*, 1013–1026. [CrossRef] [PubMed]
36. North, B.; Lehmann, A.; Dunbrack, R.L., Jr. A New Clustering of Antibody CDR Loop Conformations. *J. Mol. Biol.* **2011**, *406*, 228–256. [CrossRef]
37. Martin, A.C.; Thornton, J.M. Structural Families in Loops of Homologous Proteins: Automatic Classification, Modelling and Application to Antibodies. *J. Mol. Biol.* **1996**, *263*, 800–815. [CrossRef] [PubMed]
38. Stanfield, R.L.; Zemla, A.; Wilson, I.A.; Rupp, B. Antibody Elbow Angles Are Influenced by Their Light Chain Class. *J. Mol. Biol.* **2006**, *357*, 1566–1574. [CrossRef]
39. Bailey, L.J.; Sheehy, K.M.; Dominik, P.K.; Liang, W.G.; Rui, H.; Clark, M.; Jaskolowski, M.; Kim, Y.; Deneka, D.; Tang, W.-J.; et al. Locking the Elbow: Improved Antibody Fab Fragments as Chaperones for Structure Determination. *J. Mol. Biol.* **2018**, *430*, 337–347. [CrossRef] [PubMed]
40. Gerhardt, S.; Abbott, W.M.; Hargreaves, D.; Pauptit, R.A.; Davies, R.A.; Needham, M.R.C.; Langham, C.; Barker, W.; Aziz, A.; Snow, M.J.; et al. Structure of IL-17A in Complex with a Potent, Fully Human Neutralizing Antibody. *J. Mol. Biol.* **2009**, *394*, 905–921. [CrossRef]
41. Ekimova, V.; Ulitin, A.; Evdokimov, S.; Sofronova, E.; Nemankin, T.; Solovyev, V.; Ustugov, I.; Nedorubov, A.; Chernykh, Y.; Goncharova, O.; et al. High Affinity Anti-Il-17a Monoclonal Antibody. In Proceedings of the Conference: PEGS, Boston, MA, USA, 4–8 May 2015.
42. Padova, D.; Gram, H.; Hofstetter, H.; Jeschke, M.; Rondeau, J.; Van Den Berg, W. IL-17 Antagonistic Antibodies. U.S. Patent 7,807,155 B2, 5 October 2010.